Biosensors and Bioelectronics 91 (2017) 449–455

Contents lists available at ScienceDirect

Biosensors and Bioelectronics

journal homepage: www.elsevier.com/locate/bios

A new endoplasmic reticulum-targeted two-photon fluorescent probe for imaging of superoxide anion in diabetic mice

Haibin Xiao, Xiao Liu, Chuanchen Wu, Yaohuan Wu, Ping Li*, Xiaomeng Guo, Bo Tang*

College of Chemistry, Chemical Engineering and Materials Science, Institute of Biomedical Sciences, Collaborative Innovation Center of Functionalized Probes for Chemical Imaging in Universities of Shandong, Key Laboratory of Molecular and Nano Probes, Ministry of Education, Shandong Provincial Key Laboratory of Clean Production of Fine Chemicals, Shandong Normal University, Jinan 250014, PR China

ARTICLE INFO

Keywords:
Endoplasmic reticulum
Fluorescent probe
Superoxide anion
Diabetes
Two-photon
Imaging

ABSTRACT

Excessive or unfolded proteins accumulation in endoplasmic reticulum (ER) will cause ER stress, which has evolved to involve in various metabolic diseases. In particular, ER stress plays an important role in the pathogenesis of diabetes. Both ER stress and course of diabetes accompany oxidative stress and production of reactive oxygen species (ROS), among which superoxide anion ($O_2^{\bullet-}$) is the first produced ROS and has been recognized as cell signaling mediator involved in the physiological and pathological process of diabetes. Hence, the development of effective monitoring methods of $O_2^{\bullet-}$ in live cells and in vivo is of great importance for ascertaining the onset and progress of related diseases. Herein, a new endoplasmic reticulum-targeted two-photon fluorescent probe termed **ER-BZT** is designed and synthesized for imaging of $O_2^{\bullet-}$. The probe **ER-BZT** shows high sensitivity, selectivity, stability, and low cytotoxicity. Based on these superior properties, the rise of $O_2^{\bullet-}$ levels in endoplasmic reticulum induced with different stimuli is visualized by one- and two-photon fluorescence imaging. Most importantly, by utilizing **ER-BZT**, the two-photon fluorescence imaging results demonstrate that the endogenous $O_2^{\bullet-}$ concentration in abdominal or hepatic tissue of diabetic mice is higher than that in normal mice. Meanwhile, after treated with metformin, a broad-spectrum antidiabetic drug, the diabetic mice exhibit depressed $O_2^{\bullet-}$ level. The proposed two-photon probe, **ER-BZT** might serve as perfect tool to image the $O_2^{\bullet-}$ fluctuations and study the relevance between $O_2^{\bullet-}$ and various diseases in live cells and in vivo.

1. Introduction

Endoplasmic reticulum (ER) is the essential organelle in eukaryotic cells involving in proteins synthesizing, processing, as well as calcium storage and regulated release (Wang and Kaufman, 2014). Excessive or inaccurate protein folding in the ER may result in ER stress (Hotamisligil, 2010). Mounting evidence suggests that ER stress is closely connected to many metabolic diseases, such as diabetes, obesity, and insulin resistance (Cnop et al., 2012; Eizirik et al., 2008; Harding and Ron, 2002; Lupachyk et al., 2013; Özcan et al., 2004), which will induce production of reactive oxygen species (ROS). Notably, diabetic complications, such as hepatic disease (El-serag et al., 2004), neurodegenerative disease (Barber, 2003), nephropathy (Lewis et al., 1993) and so on are vital problems occurring in diabetic patients. Therefore, elucidating the precise mechanisms of onset and development of diabetes is one of the hotspots and difficulties in biology and medicine. There is increasing evidence that increased ROS generation may be involved in the proceeding of diabetes and corresponding complications (Dandona et al., 1996; Nishikawa and Araki, 2007). Consequently, to track the superoxide anion ($O_2^{\bullet-}$) level in ER and in diabetic mice with in situ and real time method is highly imperative for revealing the pathogenesis of diabetes and searching the potential therapeutic target.

Fluorescence imaging is a promising and powerful means for monitoring various bioactive molecules in living systems (Aron et al., 2015; Chan et al., 2012; Chen et al., 2016; Cotruvo Jr et al., 2015; Jung et al., 2016; Lee et al., 2015; Liang et al., 2014; Lin et al., 2015; Tang et al., 2015; Ueno and Nagano, 2011; Yang et al., 2016; Yin et al., 2015; Yuan et al., 2013a, 2013b). Specifically, two-photon fluorescence microscopy imaging is a fascinating approach utilizing near-infrared laser pulses, which exhibits lots of merits including deeper tissue penetration, higher spatial resolution with minimum background emission, and longer observation time (Alam et al., 2014; Helmchen and Denk, 2005). So in recent years, mounting two-photon imaging probes have been constructed for a variety of biologically active molecules (Kim and Cho, 2009, 2011, 2015; Qian et al., 2016).

* Corresponding authors.
E-mail address: tangb@sdnu.edu.cn (B. Tang).

http://dx.doi.org/10.1016/j.bios.2016.12.068
Received 22 November 2016; Received in revised form 29 December 2016; Accepted 30 December 2016
Available online 31 December 2016

Furthermore, some fluorescent probes for $O_2^{\bullet-}$ have been successfully developed (Gao et al., 2007, 2014; Henderson and Chappell, 1993; Hu et al., 2015; Li et al., 2013, 2017, 2016; Maeda et al., 2005, 2007; Robinson et al., 2006; Zhang et al., 2013, 2015; Zhao et al., 2003). For example, Yang's group reported series of highly sensitive $O_2^{\bullet-}$ sensors based on cleavage of an aryl trifluoromethanesulfonate group and achieved the detection of endogenous superoxide in live cells and in zebrafish (Hu et al., 2015). Tian's group described a ratiometric fluorescent biosensor for $O_2^{\bullet-}$ by combining carbon dots with hydroethidine, which realized imaging of $O_2^{\bullet-}$ changes upon oxidative stress in live cells (Gao et al., 2014). Our group has constructed several $O_2^{\bullet-}$-specific fluorescent probes based on the specific reaction of caffeic acid or benzothiazoline molecules to $O_2^{\bullet-}$, which fulfills the dynamic and reversible as well as mitochondria-targeted two-photon fluorescence imaging of $O_2^{\bullet-}$(Gao et al., 2007; Li et al., 2013; Zhang et al., 2013, 2015). Nevertheless, up to now, fluorescent probe for sensing of $O_2^{\bullet-}$ in ER, especially possessing two-photon absorption property hasn't been presented.

To solve the above-mentioned problems, we designed and synthesized a new two photon fluorescent probe, termed **ER-BZT** for detection of $O_2^{\bullet-}$ with excellent ER-targetability. As shown in Scheme 1, **ER-BZT** consists of 1,8-naphthalimide (a potent two-photon fluorophore), benzothiazoline (the $O_2^{\bullet-}$ recognition unit), and methyl sulphonamide (ER-targetable moiety). Benzothiazoline was utilized as the selective responsive group resulting from the transfer dehydrogenation reaction toward $O_2^{\bullet-}$(Gao et al., 2007; Li et al., 2013). The fluorescence of probe will be quenched through a photoinduced electron transfer (PET) mechanism. After dehydrogenation reaction of benzothiazoline with $O_2^{\bullet-}$, the PET process was inhibited and resulted in the recovery of the fluorescence. The experimental results demonstrated **ER-BZT** displays excellent merits including high sensitivity and selectivity, eminent ER-targetable ability, and low cytotoxicity. By utilizing this probe, we visualized the production of the $O_2^{\bullet-}$ within ER in different cells under the condition of ER stress. Above all, **ER-BZT** is successfully used to study the difference of endogenous $O_2^{\bullet-}$ concentration in normal, diabetic and metformin-treated diabetic mice.

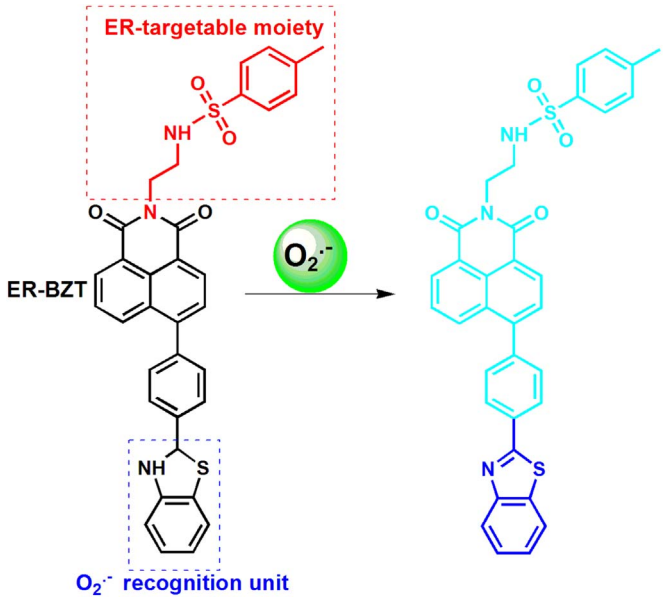

Scheme 1. The structure of **ER-BZT** and proposed reaction mechanism to $O_2^{\bullet-}$.

2. Material and methods

2.1. Reagents and instruments

Details for the reagents and apparatus used in the studies can be found in the Supplementary Information.

2.2. Preparation of various ROS

$O_2^{\bullet-}$ was prepared by dissolving KO_2 in DMSO solution. The concentration of $O_2^{\bullet-}$ was determined by various concentrations of KO_2 (Si et al., 2015); *Tert*-butyl hydroperoxide (TBHP) was delivered from 5% aqueous solutions; NaOCl solution was diluted appropriately in 0.1 M NaOHaq. The concentration of OCl^- was determined based on the molar extinction coefficient at 292 nm (350 M^{-1} cm^{-1}); H_2O_2 was diluted appropriately in water. The concentration of H_2O_2 was determined based on the molar extinction coefficient at 240 nm (43.6 M^{-1} cm^{-1}); Hydroxyl radical ($^{\bullet}OH$) was produced by Fenton reaction (Fe^{2+}/H_2O_2=1:10), and the concentration of $^{\bullet}OH$ was equal to the Fe(II) concentration (Peng et al., 2014); $^1O_2$ was generated by the addition of NaOCl and H_2O_2; Peroxynitrite ($ONOO^-$) was chemically provided by H_2O_2 and $NaNO_2$. The concentration of $ONOO^-$ was estimated by using an extinction coefficient of 1670 M^{-1} cm^{-1} (302 nm); Nitric oxide (NO) was generated from SNP (Sodium Nitroferricyanide (III) Dihydrate).

2.3. Cells culture

Human cervical cancer celss (HeLa), Human hepatoma cells (HepG2) and mice macrophages (RAW 246.7) were cultured in high glucose DMEM (4.5 g of glucose/L) supplemented with 10% fetal bovine serum, 1% penicillin, and 1% streptomycin at 37 °C in a 5% CO_2 / 95% air incubator MCO-15AC (SANYO, Tokyo, Japan). One day before imaging, the cells were detached and were replanted on glass-bottomed dishes.

2.4. General procedure for the fluorescence spectrum detection

ER-BZT was dissolved in dimethyl sulfoxide (DMSO) to produce 1.0 mM stock solution. The solution of the probe **ER-BZT** (10 μM) in 10 mM Tris-HCl buffer (pH 7.4) with 10% DMSO was obtained by diluting the probe stock solution with double-distilled water. The fluorescence spectra were recorded immediately after appropriate testing species were mixed with the probe. Unless otherwise noted, for all the measurements, the excitation wavelength is 360 nm, and the excitation/emission slit widths are 3/3 nm.

2.5. The calculation of the limit of detection

The detection limit was calculated from the fluorescence titration data. So the detection limit was calculated with the following equation: Detection limit=3σ/k, where σ is the standard deviation of blank measurement, k is the slop between the fluorescence intensity versus $O_2^{\bullet-}$ concentration.

2.6. Measurement of one-photon relative fluorescence quantum yield and two-photon cross section

Fluorescence quantum yield was determined by using quinine sulfate (Φ_f=0.55 in 0.1 mol/L H_2SO_4 excited at 365 nm) for **ER-BZT** as a fluorescence standard (Fletcher, 1969; Oushiki et al., 2010; Yuan et al., 2012). The quantum yield was calculated using the following equation:

$$\Phi_x = \Phi_s(A_sF_x/A_xF_s)(n_x/n_s)^2$$

Where Φ_x is the fluorescence quantum yield, A is the absorbance at the

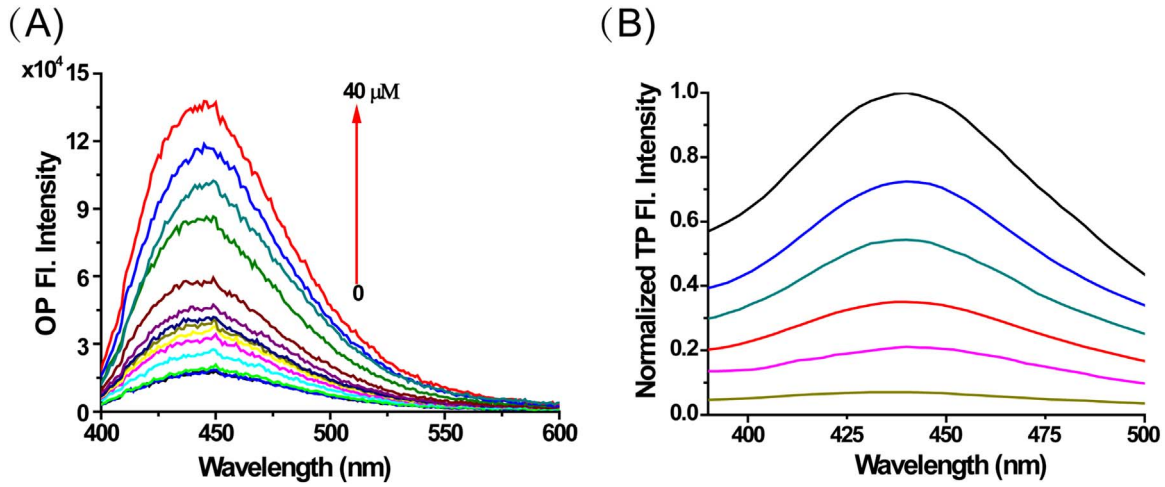

Fig. 1. (A) The one-photon (OP) fluorescence spectra of **ER-BZT** (10 μM) to different concentrations of $O_2^{\bullet-}$(0–40 μM) in Tris-HCl buffer, pH 7.4. Ex=360 nm. (B) The two-photon (TP) fluorescence response of **ER-BZT** (10 μM) to 0–40 μM of $O_2^{\bullet-}$ in Tris-HCl buffer, pH 7.4. Ex=700 nm.

excitation wavelength, F is the area under the corrected emission curve, and n is the refractive index of the solvents used. Subscripts S and X refer to the standard and to the unknown, respectively. For **ER-BZT** and quinine sulfate, the excitation wavelength was at 365 nm while keeping the absorption below 0.05.

The two-photon absorption (TPA) cross section (δ) was measured by using femto second fluorescence method (Makarov et al., 2008). **ER-BZT** were dissolved in 10 mM Tris buffer at the concentration of 10 μM and then the two-photon induced fluorescence intensity was measured at 750 nm by using fluorescein as the reference. The intensities of the two-photon induced fluorescence spectra of the reference and sample emitted at the same excitation wavelength were determined. The TPA cross section was calculated by using $\delta=\delta_r(F_s\Phi_r n_r C_r)/(F_r\Phi_s n_s C_s)$, where the subscripts s and r refer to the sample and the reference material, respectively. δ is the TPA cross sectional value, C is the concentration of the solution, n is the refractive index of the solution, F is two-photon excited fluorescence integral intensity and Φ is the fluorescence quantum yield.

2.7. Two-photon fluorescence imaging in mice

The mice were intraperitoneally injected with streptozotocin (STZ) freshly dissolved in 0.01 mol/L citrate buffer (pH 4.5) at a dose of 150 mg/kg body weight (BW) after overnight fasting. The diabetes of mouse was confirmed by the presence of hyperglycemia (blood glucose level ≥16.7 mmol/L) 72 h after STZ injection. After obtained the diabetic mice successfully, we divided the diabetic mice into three groups. **STZ group**: diabetic mice intraperitoneally injected with 100 μL saline solution once daily were used as STZ group. **STZ +Tiron group**: diabetic mice intraperitoneally injected with 100 μL trion saline solution at a dose of 150 mg/kg BW once daily were used as STZ+Tiron group. **STZ+Metf group**: diabetic mice treated with oral gavage of 100 μL metformin (Metf) saline solution at a dose of 200 mg/kg BW once daily were used as STZ+Metf group. **Normal group**: control mice intraperitoneally injected with 100 μL saline solution were used as normal group. Mice were fed regular chow and water ad libitum and maintained under the standard conditions of 30–50% relative humidity and 24–26 °C. In seventh day after treatment, mice were anesthetized with chloral hydrate, the mice were injected 100 μL of **ER-BZT** (100 μM, 10% DMSO) into abdominal cavity, then the abdominal cavity was imaged with two-photon confocal laser scanning microscopy with a 750 nm laser. For liver tissue imaging, the liver tissue was surgically exposed. Subsequently, 50 μL of **ER-BZT** (100 μM, 10% DMSO) was injected into the liver tissue, then the liver tissue was imaged with two-photon confocal laser scanning microscopy with a 750 nm laser.

3. Results and discussion

3.1. Synthesis of the probe *ER-BZT*

The synthesis of the probe is relatively facile. Compound **ER-NapBr** has been previously synthesized in our lab (Xiao et al., 2016). A Suzuki cross-coupling reaction between **ER-NapBr** and 4-formylphenylboronic acid obtained compound **ER-NapCHO**. Lastly, a reaction of **ER-NapCHO** with 2-amino thiophenol in moderate condition formed the probe **ER-BZT** (Scheme S1). The detailed synthetic routes of **ER-BZT** are provided in the Supplementary Information. The new compound and probe are well characterized with ^{1}H NMR, ^{13}C NMR and HR-MS.

3.2. The photophysical properties of the probe *ER-BZT*

Firstly, we tested the optical properties of **ER-BZT** to $O_2^{\bullet-}$ under physiological condition (10 mM Tris-HCl buffer, pH 7.4). As shown in Fig. S1, the probe displays a distinct absorption maximum peak at 375 nm. Upon addition of different concentrations of $O_2^{\bullet-}$, the intensity at 375 nm increased slightly. However, in stark contrast, the fluorescence intensity of **ER-BZT** enhanced dramatically by addition of $O_2^{\bullet-}$, showing a maximum emission peak at 450 nm (Fig. 1A). This data further verified that dehydrogenation reaction between benzothiazoline and $O_2^{\bullet-}$ abolished the PET process and enhanced the fluorescence of the probe. There is an about 11-fold fluorescence enhancement upon addition of 40 μM $O_2^{\bullet-}$, and the fluorescence quantum yield increased from 0.012 to 0.19. A good linear response was obtained between the fluorescence intensity at 450 nm and the concentrations of $O_2^{\bullet-}$ in the range of 0.1–15 μM with a detection limit of 60 nM (Fig. S2). In the meantime, **ER-BZT** can be easily excited by 700 nm laser (two-photon, TP) and exhibited marked fluorescence enhancement in the presence of increasing concentrations of $O_2^{\bullet-}$ (Fig. 1B). The two-photon absorption cross section (δ) was determined to be 65 GM. All these results indicate that **ER-BZT** could detect $O_2^{\bullet-}$ with high sensitivity by one-photon or two-photon excitation.

Next, we prove the selectivity of **ER-BZT** to $O_2^{\bullet-}$. As expected, other common ROS, including hydrogen peroxide (H_2O_2), singlet oxygen ($^1O_2$), nitric oxide (NO), *tert*-butyl hydroperoxide (TBHP), hypochlorite (OCl^-), hydroxyl radical ($^{\bullet}OH$) and peroxynitrite ($ONOO^-$) didn't induce distinguishable fluorescence intensity increase (Fig. 2A). Similarly, some metal ions also didn't influence the fluorescence intensity of **ER-BZT** (Fig. 2B). Nevertheless, obvious rise of **ER-**

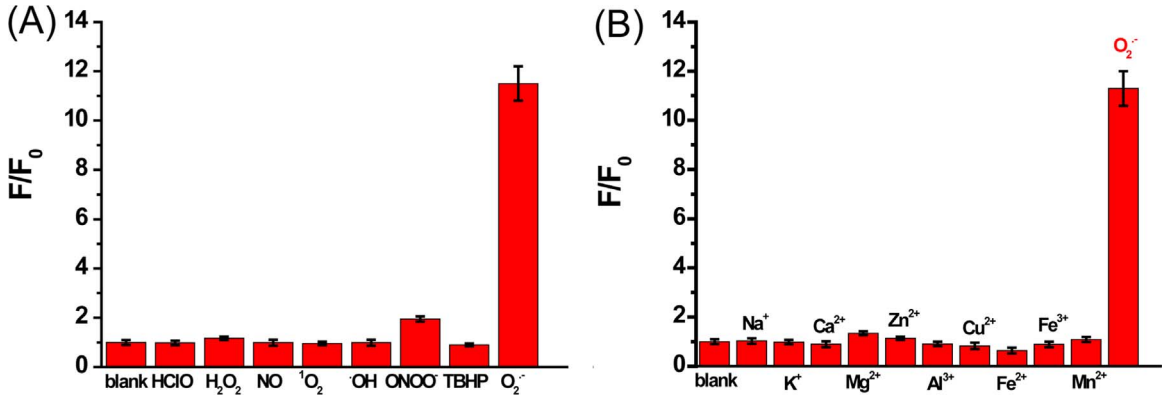

Fig. 2. (A) The fluorescence responses of **ER-BZT** (10 μM) to various ROS in Tris-HCl buffer, pH 7.4. The respective concentration of ROS is: $O_2^{\bullet-}$, 40 μmol/L; H_2O_2, 20 mmol/L; TBHP, 200 μmol/L; NaClO, 200 μM; $^1O_2$, 200 μmol/L; OH, 200 μmol/L; NO, 200 μmol/L; $ONOO^-$, 40 μmol/L. (B) The fluorescence responses of **ER-BZT** (10 μM) to various metal ions in Tris-HCl buffer, pH 7.4. The respective concentration of metal ions is: Na^+, 10 mmol/L; K^+, 10 mmol/L; Ca^{2+}, 0.5 mmol/L; Mg^{2+}, 0.5 mmol/L; Zn^{2+}, 0.5 mmol/L; Al^{3+}, 0.1 mmol/L; Cu^{2+}, 0.1 mmol/L; Fe^{3+}, 0.1 mmol/L; Fe^{2+}, 0.1 mmol/L; Mn^{2+}, 0.1 mmol/L; $O_2^{\bullet-}$, 40 μmol/L. F represents the fluorescence of **ER-BZT** in the presence of corresponding analyte, and F_0 indicates the blank fluorescence of **ER-BZT** alone.

BZT fluorescence intensity was witnessed upon $O_2^{\bullet-}$ was mixed with the probe. What's more, the fluorescence intensity of the probe before and after reaction with $O_2^{\bullet-}$ was highly stable (Fig. S3). And the pH values didn't affect the fluorescence response of **ER-BZT** to $O_2^{\bullet-}$, especially in the range of 5.0–8.0 (Fig. S4). Moreover, MTT assay displayed that **ER-BZT** has low cytotoxicity (Fig. S5). Thus, these data clearly suggested that **ER-BZT** is highly selective to $O_2^{\bullet-}$ and has excellent photostability and biocompatibility.

3.3. The subcellular localization experiment of the probe *ER-BZT*

Subsequently, to explore whether **ER-BZT** can target ER effectively, colocalization experiments were carried out in macrophages with **ER-BZT** and a commercial ER-specific fluorescent dye, ER-Tracker Red. In order to elevate the $O_2^{\bullet-}$ level in ER, we chose tunicamycin (Tm) to cause the accumulation of proteins or lipids in the ER, leading to acute ER stress and producing ROS (Nakagawa et al., 2000). Upon addition of Tm, the one-photon fluorescence of **ER-BZT** in the living cells gradually increased, indicating the rise of $O_2^{\bullet-}$ level (Fig. S6A-B). Meanwhile, the green fluorescence of **ER-BZT** overlapped well with red fluorescence obtained using ER-Tracker Red, with a Pearson's colocalization coefficient of 0.86. What's more, the brightness of stain **ER-BZT** against that of ER-Tracker Red for each pixel was plotted. The dependent staining resulted in a highly correlated plot (Fig. S6C). Further one-photon fluorescence colocalization findings were obtained in HepG2 cells by utilizing **ER-BZT** (Fig. 3A-E). Meanwhile, when Tiron, a membrane-permeable superoxide scavenger (Liao et al., 2000) was added into Tm-induced HepG2 cells, the fluorescence signal was attenuated (Fig. 3F), verifying the specificity of the probe. In addition, ER-BZT was utilized to two-photon fluorescence imaging within HepG2 cells. As illustrated in Fig. S7-S8, upon stimulated with Tm, HepG2 cells showed apparently increased two-photon fluorescence and principally distributed in ER. All these experiments demonstrate that **ER-BZT** can preferentially accumulate in ER with the help of methyl sulphonamide structure (McMahon, et al., 2013; Xiao et al., 2016) and visualize endogenous $O_2^{\bullet-}$.

3.4. The one- and two-photon fluorescence imaging of $O_2^{\bullet-}$ in ER of live cells under different stimuli

Inspired by the favorable results of live cells stained with the probe **ER-BZT**, we intended to further explore the changes in $O_2^{\bullet-}$ concentration during ER-stress initiated by other agents. So **ER-BZT** was applied to two-photon fluorescence imaging of $O_2^{\bullet-}$ level during cisplatin-induced cancer cell apoptosis process. Cisplatin is one of the most effective broad-spectrum anticancer drugs. According to widely accepted point of view, cisplatin exerts its anti-cancer activity by inducing DNA damaging apoptosis in replicating cells (Dasari and Tchounwou, 2014; Galluzzi et al., 2012). Meanwhile, mounting evidence suggested that ER stress is associated with the cisplatin-induced cell death, which supplies new strategy of promoting cisplatin chemotherapeutic efficiency by targeting endoplasmic reticulum stress (Mandic et al., 2003; Wu et al., 2011; Xu et al., 2014). As illustrated in Fig. 4, the green fluorescence of HepG2 cells exhibited obvious increase during apoptosis process induced by cisplatin. This experiment revealed that $O_2^{\bullet-}$ will be produced in ER when cancer cells were stimulated with cisplatin. Similarly, the concentration of $O_2^{\bullet-}$ will also rise in HeLa cells treated with cisplatin (Fig. S9). In addition, the one-photon fluorescence imaging results in HepG2 cells further confirmed the proposed coclusion (Fig. S10). What' more, previous studies reported that mitochondrial dysfunction may lead to increase of $O_2^{\bullet-}$ level produced from the endoplasmic reticulum surface in yeast (Leadsham et al., 2013). Interestingly, with **ER-BZT**, we also observed distinguishable enhancement of the $O_2^{\bullet-}$ level in HepG2 cells treated with carbonyl cyanide m-chlorophenylhydrazone (CCCP) that is an uncoupler of mitochondrial photophosphorylation (Goldsby and Heytler, 1963; Heytler, 1963) and can induce mitochondrial damage (Fig. S11). All the data imply that **ER-BZT** is an excellent fluorescent probe that can detect the $O_2^{\bullet-}$ level during ER stress caused by different stimuli by one- or two-photon excitation wavelengths.

3.5. The two-photon fluorescence imaging of $O_2^{\bullet-}$ in diabetic mice

It is widely accepted that enhanced oxidative stress is presented in diabetic animal model, which may contribute to the pathogenesis of diabetic complication (Desco et al., 2002; Matsumoto et al., 2003). To further explore the $O_2^{\bullet-}$ changes in normal, diabetic mice as well as drug-treated diabetic mice, we performed two-photon fluorescence imaging using **ER-BZT** in tissue of mice. To obtain diabetic mice, we utilized streptozotocin (STZ), an analog of N-acetylglucosamine, which is a specific toxin for the pancreatic beta cell and can be used for preparing diabetes animal (Burkart et al., 1999). And for simulating drug treatment modes, diabetic mice were orally treated with metformin (Metf) that is a biguanide derivate used as an oral hypoglycaemic drug in diabetics, which has protective effects on the liver injury of streptozotocin-diabetic rats (Yanardag et al., 2005). All the mice were divided into four groups: blank control mice without stimulus (Normal), STZ-induced diabetic mice (STZ), Trion-treated STZ diabetic mice (STZ+Trion), and Metf-treated STZ diabetic mice (STZ+Metf). After anaesthetized, the liver of the mice was surgically exposed and injected with ER-BZT (100 μM, 50 μL, 10% DMSO). Subsequently, we carried out the two-photon fluorescence imaging of the liver tissue with

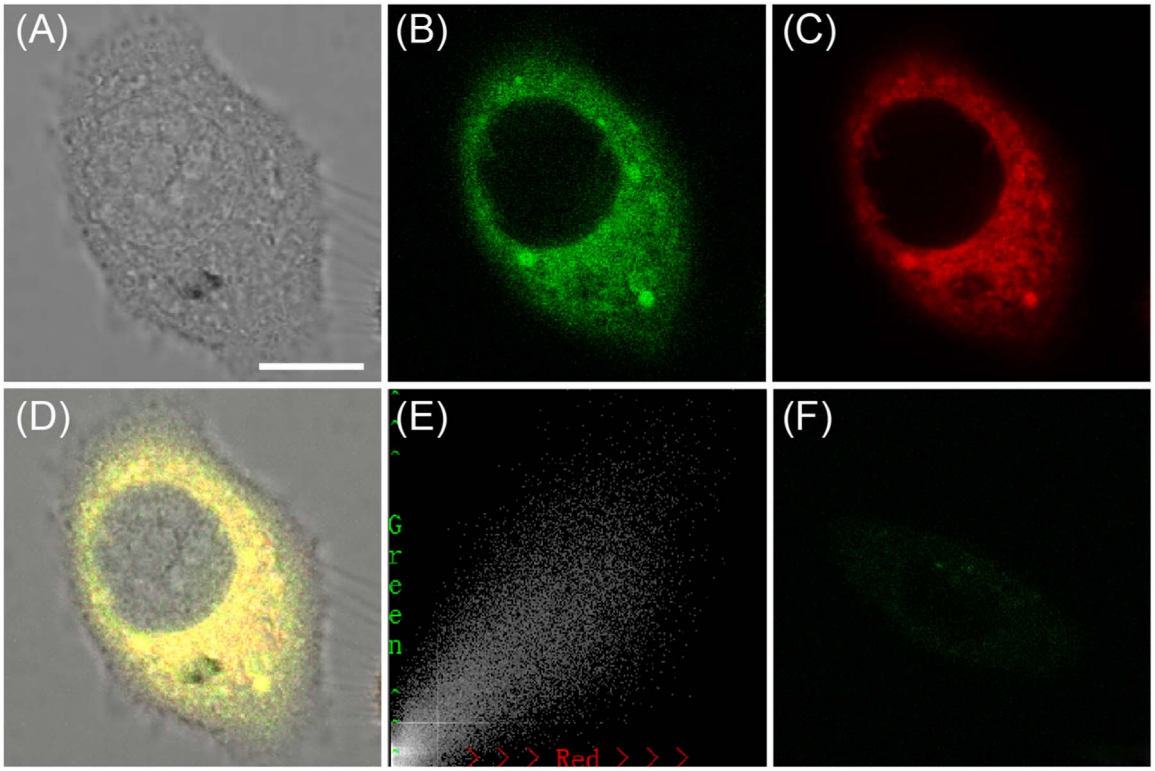

Fig. 3. The colocalization imaging of **ER-BZT** and ER-tracker Red in Tm-treated HepG2 cells (A) The bright-field image. (B) The fluorescence image of **ER-BZT** (10 μM, Ex=405 nm, collected 420–480 nm). (C) The fluorescence image of ER-Tracker Red (0.5 μM, Ex=543 nm, collected 580–630 nm). (D) The merged image of A-C. (E) Intensity correlation plot of stain **ER-BZT** and ER-Tracker Red. (F) The fluorescence image of **ER-BZT** in Tm-induced HepG2 cells pretreated with Tiron (5.0 mM) for 20 min. Scale bar: 10 μm.

750 nm two-photon laser. As illustrated in Fig. 5, the 3D stack images demonstrated that the fluorescence intensity in liver tissue of STZ diabetic mice (STZ) was obvious higher than that in normal mice (Normal), indicating that liver tissue in diabetic mice displayed enhanced oxidative stress and possessed higher $O_2^{\bullet-}$ level. To further confirm the higher $O_2^{\bullet-}$ concentration in liver tissue of diabetic mice, Tiron was injected into the liver of STZ-induced diabetic mice (STZ +Tiron). After pretreated with Tiron, the liver tissue of diabetic mice showed faint fluorescence intensity, suggesting the elimination of $O_2^{\bullet-}$ and verifying the specificity of the probe. Additionally, after oral gavage of Metf daily (100 μL) for 7 days, the liver tissue of STZ diabetic mice (STZ+Metf) displayed lower fluorescence intensity compared to the STZ diabetic mice. This result indicated that the Metf-treated STZ diabetic mice had lower $O_2^{\bullet-}$ concentration in liver tissue. Presumably, this is because Metf, as a widely used antihyperglycemic drug can lower the glucose level and ameliorate the oxidative stress during diabetes. The similar result was obtained in abdominal tissue imaging utilizing **ER-BZT** (Fig. S12). The abdominal tissue in diabetic mice possessed higher $O_2^{\bullet-}$ level, and the elevated $O_2^{\bullet-}$ concentration declined distinctly after treatment with Metf. These results obtained by the proposed two-photon fluorescence visualization method were in accordance with previous work detected by electron spin resonance (ESR) spectroscopy (Kakkar et al., 1998; Sano et al., 1998). These data further illustrate that **ER-BZT** is an ideal fluorescence imaging tool for two-photon visualization of $O_2^{\bullet-}$ difference in abdominal and hepatic tissue of normal/diabetic mice.

4. Conclusions

In conclusion, we have developed a new two-photon fluorescent probe for imaging of $O_2^{\bullet-}$ in endoplasmic reticulum. The probe **ER-BZT** can respond to changes in $O_2^{\bullet-}$ levels sensitively and selectively. **ER-BZT** also exhibits excellent photostability, low cytotoxicity and insensitive to pH changes. In contrast with some previous $O_2^{\bullet-}$ probes, **ER-BZT** displays comparable properties, including facile synthesis, low detection limit (60 nM), fast response time (within seconds), excellent and first ER-targetable ability and one/two photon absorption. In view of the favorable merits, **ER-BZT** was successfully used to spy $O_2^{\bullet-}$ burst under the condition of endoplasmic reticulum stress induced by Tm, CCCP and cisplatin through confocal fluorescence imaging. Above all, by using **ER-BZT** in vivo two-photon fluorescence imaging, it's found that endogenous $O_2^{\bullet-}$ level in abdominal and

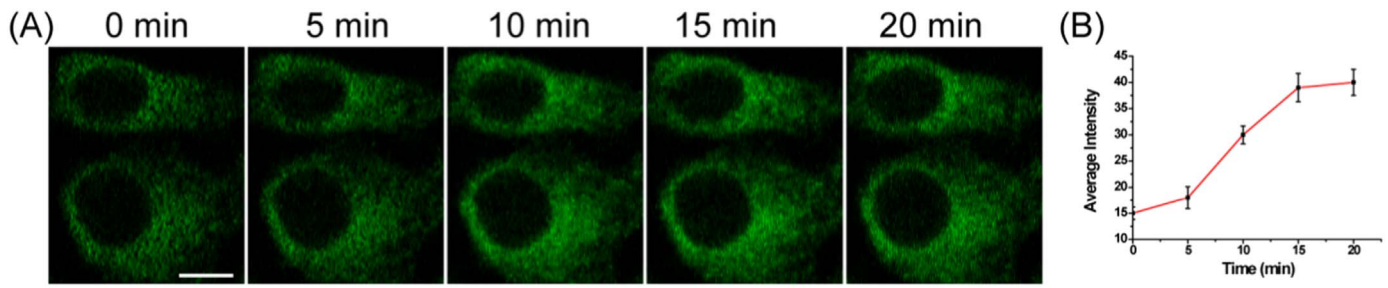

Fig. 4. The two-photon fluorescence imaging of $O_2^{\bullet-}$ with **ER-BZT** in HepG2 cells stimulated with cisplatin. (A) The fluorescence images of **ER-BZT** (10 μM, Ex=750 nm, collected 420–480 nm) at different times upon addition of cisplatin (100 μM). (B) The output of average fluorescence intensity. Scale bar: 10 μm.

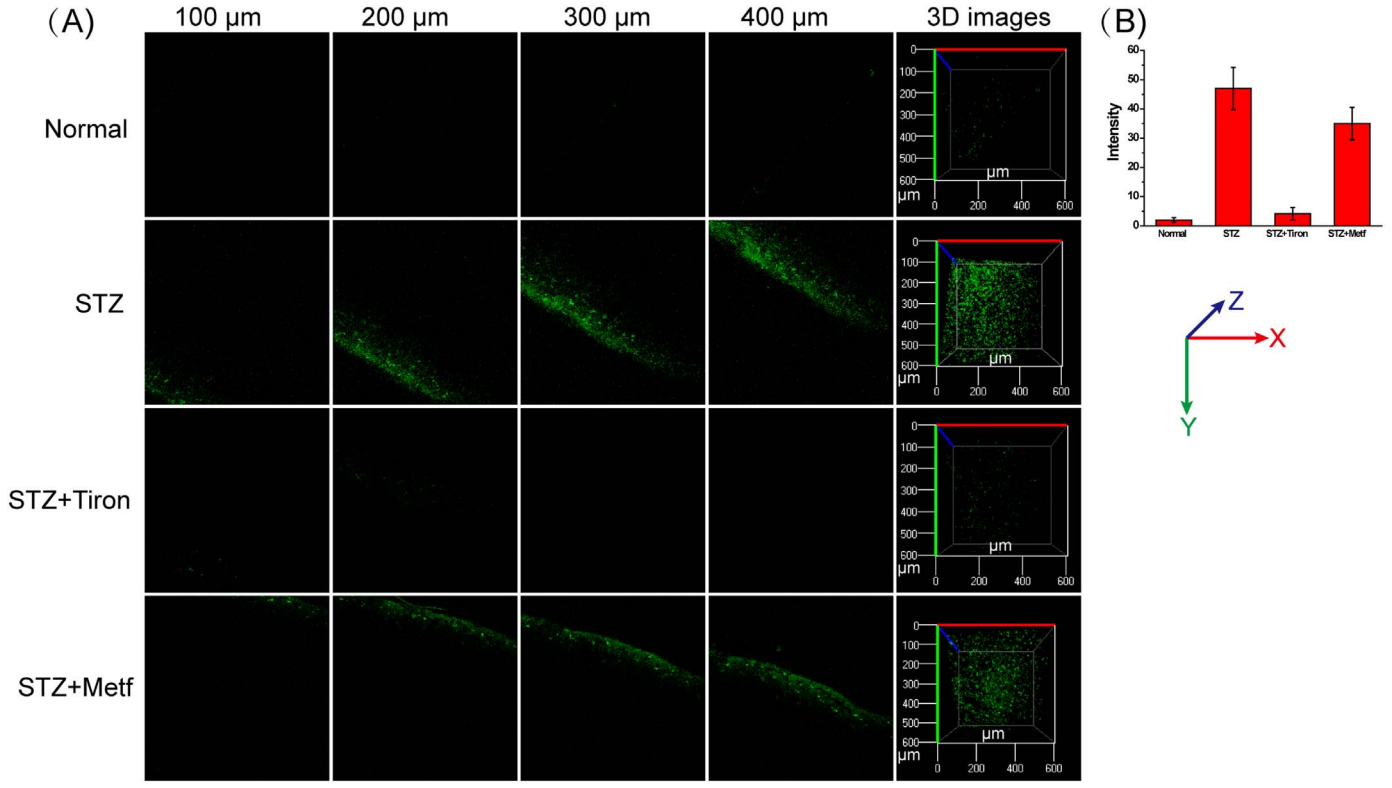

Fig. 5. The two-photon fluorescence imaging of $O_2^{\bullet-}$ in liver tissue of mice. (A) The fluorescence images of liver tissue stained with **ER-BZT** at different depths and the 3D stack images. (B) The fluorescence intensity statistics was output by selecting five representative regions. The probe concentration is 100 μM (50 μL). The two-photon laser is 750 nm, and fluorescence is collected from 420 to 480 nm.

hepatic tissue of diabetic mice is higher than that in normal mice. In the meantime, after treatment with metformin, a widely used anti-hyperglycemic drug, the production of $O_2^{\bullet-}$ in diabetic mice was ameliorated. All the data further verify that $O_2^{\bullet-}$ is inextricably linked to ER-associated disorders. The presented probe provides a powerful tool for uncovering the chemical biology roles of $O_2^{\bullet-}$ in endoplasmic reticulum-associated diseases.

Acknowledgements

This work was supported by 973 Program (2013CB933800), National Natural Science Foundation of China (21390411, 21535004 , 21475079, and 21675105), and the Program for Changjiang Scholars and Innovative Research Team in University (IRT 16R46).

Appendix A. Supporting information

Supplementary data associated with this article can be found in the online version at doi:10.1016/j.bios.2016.12.068.

References

Alam, M.M., Chattopadhyaya, M., Chakrabarti, S., Ruud, K., 2014. Acc. Chem. Res. 47, 1604–1612.
Aron, A.T., Ramos-Torres, K.M., Cotruvo, J.A., Jr, Chang, C.J., 2015. Acc. Chem. Res. 48, 2434–2442.
Barber, A.J., 2003. Prog. Neuro-Psychoph. 27, 283–290.
Burkart, V., Wang, Z.Q., Radons, J., Heller, B., Herceg, Z., Stingl, L., Wagner, E.F., Kolb, H., 1999. Nat. Med. 5, 314–319.
Chan, J., Dodani, S.C., Chang, C.J., 2012. Nat. Chem. 4, 973–984.
Chen, X., Wang, F., Hyun, J.Y., Wei, T., Qiang, J., Ren, X., Shin, I., Yoon, J., 2016. Chem. Soc. Rev. 45, 2976–3016.
Cnop, M., Foufelle, F., Velloso, L.A., 2012. Trends Mol. Med. 18, 59–68.
Cotruvo, J.A., Jr, Aron, A.T., Ramos-Torres, K.M., Chang, C.J., 2015. Chem. Soc. Rev. 44, 4400–4414.
Dandona, P., Thusu, K., Cook, S., Snyder, B., Makowski, J., Armstrong, D., Nicotera, T., 1996. Lancet 347, 444–445.
Dasari, S., Tchounwou, P.B., 2014. Eur. J. Pharmacol. 740, 364–378.
Desco, M.C., Asensi, M., Márquez, R., Martínez-Valls, J., Vento, M., Pallardó, F.V., Sastre, J., Viña, J., 2002. Diabetes 51, 1118–1124.
Eizirik, D.L., Cardozo, A.K., Cnop, M., 2008. Endocr. Rev. 29, 42–61.
El-serag, H.B., Tran, T., Everhart, J.E., 2004. Gastroenterology 126, 460–468.
Fletcher, A.N., 1969. Photochem. Photobiol. 9, 439–444.
Galluzzi, L., Senovilla, L., Vitale, I., Michels, J., Martins, I., Kepp, O., Castedo, M., Kroemer, G., 2012. Oncogene 31, 1869–1883.
Gao, J.J., Xu, K.H., Tang, B., Yin, L.L., Yang, G.W., An, L.G., 2007. FEBS J. 274, 1725–1733.
Gao, X., Ding, C., Zhu, A., Tian, Y., 2014. Anal. Chem. 86, 7071–7078.
Goldsby, R.A., Heytler, P.G., 1963. Biochemistry 2, 1142–1147.
Harding, H.P., Ron, D., 2002. Diabetes 51, S455–S461.
Helmchen, F., Denk, W., 2005. Nat. Methods 2, 932–940.
Henderson, L.M., Chappell, J.B., 1993. Eur. J. Biochem. 217, 973–980.
Heytler, P.G., 1963. Biochemistry 2, 357–361.
Hotamisligil, G.S., 2010. Cell 140, 900–917.
Hu, J.J., Wong, N.K., Ye, S., Chen, X., Lu, M.Y., Zhao, A.Q., Guo, Y., Ma, A.C.H., Leung, A.C.H., Shen, J., Yang, D., 2015. J. Am. Chem. Soc. 137, 6837–6843.
Jung, H.S., Verwilst, P., Kim, W.Y., Kim, J.S., 2016. Chem. Soc. Rev. 45, 1242–1256.
Kakkar, R., Mantha, S.V., Radhi, J., Prasad, K., Kalra, J., 1998. Clin. Sci. 94, 623–632.
Kim, H.M., Cho, B.R., 2009. Acc. Chem. Res. 42, 863–872.
Kim, H.M., Cho, B.R., 2011. Chem. Asian J. 6, 58–69.
Kim, H.M., Cho, B.R., 2015. Chem. Rev. 115, 5014–5055.
Leadsham, J.E., Sanders, G., Giannaki, S., Bastow, E.L., Hutton, R., Naeimi, W.R., Breitenbach, M., Gourlay, C.W., 2013. Cell Metab. 18, 279–286.
Lee, M.H., Kim, J.S., Sessler, J.L., 2015. Chem. Soc. Rev. 44, 4185–4191.
Lewis, E.J., Hunsicker, L.G., Bain, R.P., Rohde, R.D., 1993. New Engl. J. Med. 329, 1456–1462.
Li, P., Liu, L., Xiao, H., Zhang, W., Wang, L., Tang, B., 2016. J. Am. Chem. Soc. 138, 2893–2896.
Li, P., Zhang, W., Li, K., Liu, X., Xiao, H., Zhang, W., Tang, B., 2013. Anal. Chem. 85, 9877–9881.
Li, R.Q., Mao, Z.Q., Rong, L., Wu, N., Lei, Q., Zhu, J.Y., Zhuang, L., Zhang, X.Z., Liu, Z.H., 2017. Biosens. Bioelectron. 87, 73–80.
Liang, H., Zhang, X., Lv, Y., Gong, L., Wang, R., Zhu, X., Yang, R., Tan, W., 2014. Acc. Chem. Res. 47, 1891–1901.
Liao, D.F., Jin, Z.G., Baas, A.S., Daum, G., Gygi, S.P., Aebersold, R., Berk, B.C., 2000. J. Biol. Chem. 275, 189–196.
Lin, V.S., Chen, W., Xian, M., Chang, C.J., 2015. Chem. Soc. Rev., 4596–4618.
Lupachyk, S., Watcho, P., Stavniichuk, R., Shevalye, H., Obrosova, I.G., 2013. Diabetes 62, 944–952.
Maeda, H., Yamamoto, K., Kohno, I., Hafsi, L., Itoh, N., Nakagawa, S., Kanagawa, N.,

Suzuki, K., Uno, T., 2007. Chem. Eur. J. 13, 1946–1954.
Maeda, H., Yamamoto, K., Nomura, Y., Kohno, I., Hafsi, L., Ueda, N., Yoshida, S., Fukuda, M., Fukuyasu, Y., Yamauchi, Y., Itoh, N., 2005. J. Am. Chem. Soc. 127, 68–69.
Makarov, N.S., Drobizhev, M., Rebane, A., 2008. Opt. Exp. 16, 4029–4047.
Mandic, A., Hansson, J., Linder, S., Shoshan, M.C., 2003. J. Biol. Chem. 278, 9100–9106.
Matsumoto, S., Koshiishi, I., Inoguchi, T., Nawata, H., Utsumi, H., 2003. Free Radic. Res. 37, 767–772.
McMahon, B.K., Pal, R., Parker, D., 2013. Chem. Commun. 49, 5363–5365.
Nakagawa, T., Zhu, H., Morishima, N., Li, E., Xu, J., Yankner, B.A., Yuan, J., 2000. Nature 403, 98–103.
Nishikawa, T., Araki, E., 2007. Antioxid. Redox Sign. 9, 343–353.
Oushiki, D., Kojima, H., Terai, T., Arita, M., Hanaoka, K., Urano, Y., Nagano, T., 2010. J. Am. Chem. Soc. 132, 2795–2801.
Özcan, U., Cao, Q., Yilmaz, E., Lee, A.H., Iwakoshi, N.N., Özdelen, E., Tuncman, G., Görgün, C., Glimcher, L.H., Hotamisligil, G.S., 2004. Science 306, 457–461.
Peng, T., Wong, N.K., Chen, X., Chan, Y.K., Ho, D.H.H., Sun, Z., Hu, J.J., El-Nezami, H., Yang, D., 2014. J. Am. Chem. Soc. 136, 11728–11734.
Qian, L., Li, L., Yao, S.Q., 2016. Acc. Chem. Res. 49, 626–634.
Robinson, K.M., Janes, M.S., Pehar, M., Monette, J.S., Ross, M.F., Hagen, T.M., Murphy, M.P., Beckman, J.S., 2006. Proc. Natl. Acad. Sci. 103, 15038–15043.
Sano, T., Umeda, F., Hashimoto, T., Nawata, H., Utsumi, H., 1998. Diabetologia 41, 1355–1360.
Si, F., Liu, Y., Yan, K., Zhong, W., 2015. Chem. Commun. 51, 7931–7934.
Tang, Y., Lee, D., Wang, J., Li, G., Yu, J., Lin, W., Yoon, J., 2015. Chem. Soc. Rev. 44, 5003–5015.
Ueno, T., Nagano, T., 2011. Nat. Methods 8, 642–645.
Wang, M., Kaufman, R.J., 2014. Nat. Rev. Cancer 14, 581–597.
Wu, Z.Z., Sun, N.K., Chien, K.Y., Chao, C.C.K., 2011. Biochem. Pharmacol. 82, 1630–1640.
Xiao, H., Li, P., Hu, X., Shi, X., Zhang, W., Tang, B., 2016. Chem. Sci. 7, 6153–6159.
Xu, Y., Wang, C.Y., Li, Z.X., 2014. Mol. Clin. Oncol. 2, 3–7.
Yanardag, R., Ozsoy-Sacan, O., Bolkent, S., Orak, H., Karabulut-Bulan, O., 2005. Hum. Exp. Toxicol. 24, 129–135.
Yang, Z., Sharma, A., Qi, J., Peng, X., Lee, D.Y., Hu, R., Lin, D., Qu, J., Kim, J.S., 2016. Chem. Soc. Rev. 45, 4651–4667.
Yin, J., Hu, Y., Yoon, J., 2015. Chem. Soc. Rev. 44, 4619–4644.
Yuan, L., Lin, W., Zhao, S., Gao, W., Chen, B., He, L., Zhu, S., 2012. J. Am. Chem. Soc. 134, 13510–13523.
Yuan, L., Lin, W., Zheng, K., He, L., Huang, W., 2013a. Chem. Soc. Rev. 42, 622–661.
Yuan, L., Lin, W., Zheng, K., Zhu, S., 2013b. Acc. Chem. Res. 46, 1462–1473.
Zhang, W., Li, P., Yang, F., Hu, X., Sun, C., Zhang, W., Chen, D., Tang, B., 2013. J. Am. Chem. Soc. 135, 14956–14959.
Zhang, W., Wang, X., Li, P., Huang, F., Wang, H., Zhang, W., Tang, B., 2015. Chem. Commun. 51, 9710–9713.
Zhao, H., Kalivendi, S., Zhang, H., Joseph, J., Nithipatikom, K., Vasquez-Vivar, J., Kalyanaraman, B., 2003. Free Radic. Biol. Med. 34, 1359–1368.